Indian Journal of Chemistry
Vol. 63, October 2024, pp. 959-972
DOI: 10.56042/ijc.v63i10.11294

Aggregation induced emissive pyrimido fused tetraphenylethene benzothiazole probe for sensitive and selective detection of Fe^{3+} ions

Dnyaneshwar I Bhusanur[a,f], Harshad A Mirgane[b], Prabhat K Singh[c,d], Mohammad Al Kobaisi[e], Sheshanath V Bhosale[b] & Sidhanath V Bhosale*[a,f]

[a] Polymers and Functional Materials Division, CSIR-Indian Institute of Chemical Technology, Hyderabad 500 007, Telangana, India

[b] Department of Chemistry, School of Chemical Sciences, Central University of Karnataka, Kadaganchi, Kalaburagi 585 367, Karnataka, India

[c] Radiation and Photochemistry Division, Bhabha Atomic Research Centre, Mumbai 400 085, India

[d] Homi Bhabha National Institute, Training School Complex, Anushaktinagar, Mumbai 400 094, India

[e] School of Science, RMIT University, GPO Box 2476, Melbourne, VIC, 3001, Australia

[f] Academy of Scientific and Innovative Research (AcSIR), CSIR-HRDC Campus, Postal Staff College Area Sector 19, Kamla Nehru Nagar, Ghaziabad 201 002, Uttar Pradesh, India

E-mail: bhosale@iict.res.in

Received 22 May 2024; accepted (revised) 30 August 2024

The synthesis and photophysical properties of a novel pyrimido fused benzothiazole-tetraphenylethene (TPE-1) chromophore, incorporating both electron-donating ($–SCH_3$) and electron-withdrawing (–CN) groups, are reported. TPE-1 exhibits aggregation-induced emission (AIE), mechanochromic, and electrochemical characteristics. The recognition behavior of TPE-1 towards various metal cations is investigated by fluorescence spectroscopy. TPE-1 shows a selective and sensitive response towards ferric (Fe^{3+}) ion over other tested cations in DMSO: water (90:10, *v/v* ratio) with a limit of detection of 102 nM. Time-correlated single photon counting (TCSPC) plot displays dynamic and static quenching of TPE-1 with the addition of Fe^{3+} ions. Computational studies have been performed to demonstrate the binding mode of TPE-1 towards Fe^{3+} ions. Most importantly, the application of TPE-1 in the detection of Fe^{3+} ions in various water sources showcases its promising utility in environmental monitoring and pollution control, underscoring its potential for substantial contributions to environmental chemistry and sensor technology.

Keywords: Benzothiazole, Tetraphenylethylene, Pyrimido, Fe^{3+} ions, Sensor

Iron (Fe^{3+}), a transition metal ion, is among the most physiologically abundant elements on Earth and plays a crucial role in biological systems[1-3]. Fe^{3+} ion plays an important role in electron transfer, oxygen metabolism and transcriptional regulations in the living systems[4-8]. Excess presence of Fe^{3+} ions chronically causes various diseases *e.g.* cancers, heart diseases, hepatitis and diabetes[9-11]. On the other hand, Fe^{3+} deficiency results into anaemia, neurobehavioral disorder such as Alzheimer's, and Parkinson's diseases[12]. Consequently, monitoring Fe^{3+} levels in the human body is a critical task for medical practitioners. Additionally, there is a growing demand for sensitive and selective detection methods for Fe^{3+} ion recognition in drinking water.A review of the literature indicates that numerous sophisticated instrumental techniques have been utilized for detecting Fe^{3+} ions[13-17]. However, these methods have their own limitations regarding result reproducibility, technique reliability, high costs, maintenance of ambient conditions, and instrument handling. To address these challenges, simpler and more reliable methods based on colorimetric and fluorescence recognition of Fe^{3+} ions have emerged as attractive alternatives. Fluorescent probes, including organic small chromophores, polymers, and quantum dots, are extensively used for sensing in chemistry and imaging in biology[18-24].These methods typically rely on "turn-on" and "turn-off" fluorescent mechanism[25-26]. However, some of these approaches exhibit disadvantages such as low photo-stability, poor water solubility, high toxicity, and the requirement for organic solvents. These drawbacks limit their practical applications in environmental and biological systems. Researchers are continuously striving to design and develop efficient, highly sensitive,

selective, and cost-effective fluorescent probes for Fe^{3+} ion detection. Recently, aggregation-induced emission (AIE) probes have been specifically designed and developed to enhance sensitivity and selectivity for Fe^{3+} ion recognition in aqueous media[27-29].AIE molecular architectures are an efficient recognition method for the colorimetric and fluorescence recognition of metal ions without employing expensive instruments[30].Therefore, the design and development of new AIE materials for recognition of selective metal ions is of significant interest. Inspired from the fascinating literature reports based on AIE materials for Fe^{3+} ion detection, we are interested to design and develop a new chromophore which could recognize Fe^{3+} ion in aqueous media.

In this study, we introduce a novel chromophore, TPE-1, which bears a unique molecular architecture, blending a benzothiazole-tetraphenylethene structure with a pyrimidine fluorophore, enhanced by strategically placed electron-donating and electron-withdrawing groups. This innovative design facilitates impressive aggregation-induced emission (AIE) and mechanochromic properties, setting TPE-1 distinct from existing chromophores. Moreover, TPE-1 exhibits very high sensitivity and selectivity towards ferric (Fe^{3+}) ions in aqueous environments, achieving a detection limit as low as 102 nM. This sensitivity is critical for applications in environmental monitoring and biomedical diagnostics, where precise detection of metal ions is essential. Furthermore, the reversible color change under mechanical stress opens avenues for the application of TPE-1 in developing smart materials and responsive sensors. Complementing our experimental findings, computational studies provide a deep insight into the binding interactions and stoichiometry of TPE-1 with Fe^{3+} ions, thereby offering a comprehensive understanding of its functionality. Collectively, these novel attributes of TPE-1 mark a significant contribution in the synthesis of multifunctional chromophores and pave the way for new research directions in sensing and material science.

Experimental Section

Materials and Methods

All chemicals and solvents were bought from Sigma-Aldrich and AVARA Pvt. Ltd., India and used without further purification. The reaction progress was monitored by thin-layer chromatography (TLC) and spots were visualized with short UV light. IR spectra of the synthesized compounds were measured on a Thermo Nicolet Nexus 670 spectrometer. ^{1}H and ^{13}C NMR spectra were recorded using a Bruker Avance 400 MHz and 100 MHz spectrometer, respectively. Chemical shifts were reported in parts per million shifts (δ value) from tetramethyl silane (TMS, δ scale) as internal standards with the solvent resonances. HRMS data were taken on Shimadzu lab solutions (Fig. S1 to Fig. S10). UV-Vis and Fluorescence Spectra were recorded on a Shimadzu UV-1800 spectrophotometer and RF-6000 Shimadzu Spectrofluorometer, respectively.

Synthesis of 2-(methylthio)-4-oxo-8-(1,2,2-triphenylvinyl)-4H-benzo[4,5]thiazolo[3,2-a]pyrimidine-3-carbonitrile [TPE-1]

6-(1,2,2-triphenylvinyl)benzo[d]thiazol-2-amine **1** (0.2 g, 0.49 mmol), ethyl 2-cyano-3,3-bis(methylthio)acrylate **2** (0.193 g, 0.889 mmol), potassium carbonate (0.341 g 2.47 mmol) in dry toluene (10 mL) dissolved and reaction mixture was refluxed for 12h. The progress of reaction was monitored by TLC plate. After completion, the reaction solution was cooled to r.t. The solvent was evaporated by rotary evaporation and the obtained residue was washed with water. The crude product was purified by column chromatography using a mixture of hexane: dichloromethane (1:1) as eluent to obtain compound TPE-1 as a white solid yield: 70%. FT-IR (cm^{-1} KBr) 3014, 2213, 1688, 1536, 1479, 1338, 1241, 1190, 1037, 880, 838, 766, 698; ^{1}H NMR (400 MHz, $CDCl_3$) δ ppm: 8.73-8.71 (d, J = 8.80 Hz, 1H), 7.38.7.37 (d, 1H, J = 1.589 Hz,), 7.28 (d, 1H, J=1.71 Hz), 7.16-7.11 (m, 9H), 7.04-7.01 (m, 6H), 2.64 (s, 3H); ^{13}C NMR (100 MHz, $CDCl_3$) δ 173.4, 156.9, 144.2, 143.3, 142.8, 138.6, 131.5, 131.5, 131.3, 131.2, 131.1, 128.1, 127.8, 127.2, 127.0, 127.0, 124.3, 123.3, 119.3, 113.6, 13.7; ESI-mass *m/z*: calcd 527.11 $[M]^+$, found 528 $[M+H]^+$; HRMS *m/z*: $[M+H]^+$ calcd. for $C_{32}H_{21}N_3OS_2$ 528.1198; found 528.1218.

Preparation of stock solutions

The stock solution of TPE-1 was prepared 2 x10^{-3} M in DMSO and various metal cations such as Hg^{2+}, Co^{2+}, Ni^{2+}, Ba^{2+}, Cd^{2+}, Fe^{3+}, In^{3+}, Mn^{2+}, Cr^{3+}, Mg^{2+}, Zn^{2+} and Cu^{2+} were 8 x 10^{-3} M prepared in water at room temperature respectively. As-prepared stock solutions were utilized for all UV-Vis and fluorescence spectroscopic investigation upon appropriate dilution.

UV-Vis and Fluorescence experiments

The required amount of stock solution is diluted to 3 mL of the TPE-1 receptor TPE-1 (1 x 10^{-5} M, in DMSO and DMSO: water). These samples were examined by taking directly into the cuvette for UV-Vis and fluorescence measurements as well as for the tested cations (0-80 equiv.) at room temperature.

Stern-Volmer equation

Stern–Volmer quenching constant (K_{SV}) was determined using the titration data with the help of the following Stern–Volmer equation[31].

$I_0/I = 1 + K_{SV}$

where,

I_0: Emission intensity in the absence of Fe^{3+}

I: Emission intensity in presence of Fe^{3+}

K_{SV}: Stern-Volmer Quenching constant

Limit of detection calculations

The limit of detection (LOD) was determined based on fluorescence titration experiments. The standard deviation of TPE-1 was estimated from three repeated measurements. The slopes of the calibration plot from the fluorescence intensity and the concentration of the Fe^{3+} was utilized to calculate the LOD using following equation:

$LOD = 3\sigma/S$

where σ is the standard deviation of the probe and *s* is the slope value from the calibration plot.

Thermogravimetric Analysis (TGA)

Thermogravimetric analysis (TGA) was carried out on TA Q 500 Sample and was heated up to 800°C heating rate of 10°C per minute under nitrogen gas flow. 5% weight loss at 365°C respectively.

Computational calculations

The DFT calculations were performed at B3LYP def2-SVP def2/J level of theory[32] and the CASSCF was carried out at RIJCOSX def2-SVP def2-svp/c def2/J level of theory[33].

Results and Discussion

Design and Synthesis of TPE-1

In this study, a new molecular structure, TPE-1, was designed based on an aggregation-induced emission (AIE) subunit. This structure consists of a benzothiazole-incorporated tetraphenylethylene (TPE) fused with a pyrimidine fluorophore (Fig. 1). Additionally, the inclusion of electron-donating (–SCH_3) and electron-withdrawing (–CN) functional groups on the pyrimido unit imparts distinctive photophysical characteristics. These features enable manipulation of the fluorescence properties of the chromophore in the blue region[34-35].

Synthesis of TPE-1

The condensation between 6-(1,2,2-triphenylvinyl)benzo[d]thiazol-2-amine (1)[28] and ethyl 2-cyano-3,3-bis(methylthio)acrylate (2) in the presence of oven dried K_2CO_3 in dry toluene furnished 2-(methylthio)-4-oxo-8-(1,2,2-triphenylvinyl)-4H-benzo[4,5]thiazolo[3,2-a] pyrimidine-3-carbonitrile (TPE-1) in 70% yield (Scheme 1). The FT-IR spectra of TPE-1 showed characteristic peaks of –CN at 2213 cm^{-1} and –C=O at 1688 cm^{-1} (Fig. S6 in SI). The ^1H NMR of the TPE-1

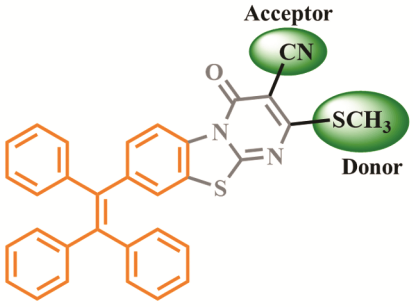

TPE-1

Fig. 1 — Design of TPE-1

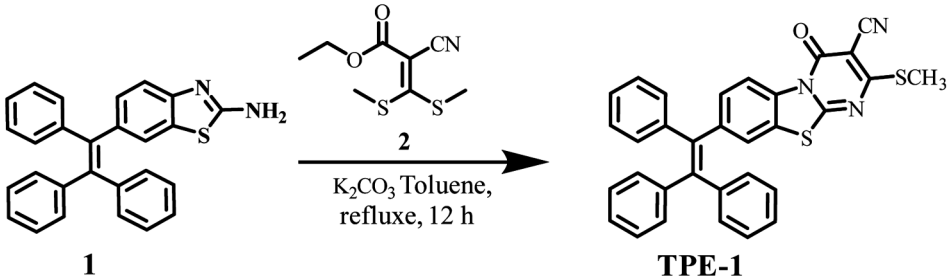

Scheme 1 — Synthetic scheme of TPE-1

displayed singlet at 2.64 ppm corresponding to –SCH_3 protons (Fig. S7, SI). The mass and HRMS spectrum of TPE-1 exhibited a molecular ion peak at m/z 528 $[M+1]^+$ (Fig. S9 in SI) and 528.1218 $[M+H]^+$ (Fig. S10 in SI), respectively. These spectroscopic data corroborate the structure of TPE-1 (Fig. 2, Scheme 1). Thermogravimetric method was employed to examine the thermal stability of TPE-1. As displayed in Fig. S11, TPE-1 exhibited 5% wt. loss at 365°C, suggesting the molecular architecture is thermally stable enough to utilize at higher temperature.

The formation of compound TPE-1 can be described with the plausible mechanism as demonstrated in Scheme 2[36].

Optical properties of TPE-1

The ultraviolet-visible (UV-Vis) absorption and fluorescence spectra of TPE-1 were evaluated in various solvents, as shown in Fig. 2. In all tested solvents, absorption peaks at approximately 335 nm were consistently observed. However, deviations were noted in specific solvents: acetonitrile showed no peak around 355 nm, and MCH exhibited peaks at 358 nm and 371 nm. In contrast, in $CHCl_3$, DMSO, and MeOH, a new absorption band emerged around 370, 366, and 365 nm, respectively (Fig. 2a). These observations suggest additional interactions between TPE-1 and the solvents in $CHCl_3$, DMSO, and MeOH. Despite these variations, the absorption maxima of TPE-1 showed negligible shifts across the tested solvents. This indicates that the electronic ground state of TPE-1 is largely independent of solvent polarity, implying an association with a low dipole moment change[37].

Fluorescence (FL) emission spectra of TPE-1 in the above solvents are shown in Fig. 2b. In MCH, TPE-1 displayed less intense peaks at 403 nm and 431 nm and the calculated quantum yield (ϕ) was found to be 2.47%. Whereas, in DMSO very weak emission peak was observed at 542 nm with quantum yield of about ϕ = 1.92%. In $CHCl_3$ and DCM, intense FL peaks are observed at 414 and 435 nm along with shoulder peak at 365 nm. The quantum yields (ϕ) of TPE-1in $CHCl_3$ and DCM found to be 24.18% and 19.26%, respectively. Similarly, ACN and MeOH exhibited FL peaks 411 nm 430 nm with significant intensity. The estimated quantum yield for TPE-1 in acetonitrile and MeOH was found to be ϕ = 5.26% and (ϕ = 3.80%), respectively. Moreover, in MeOH shoulder peak was

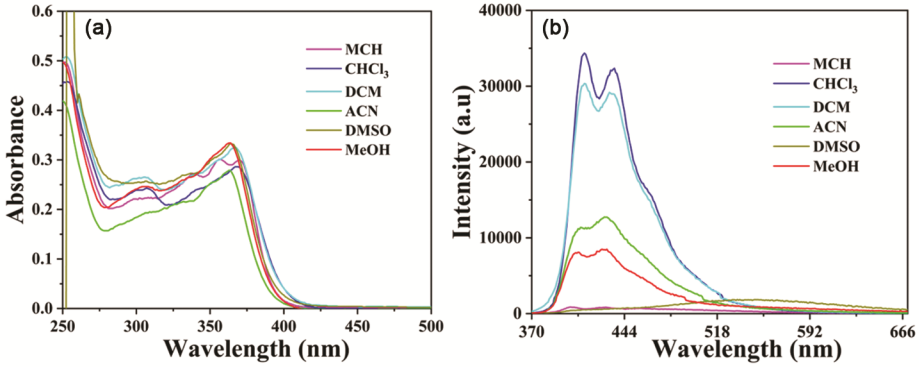

Fig. 2 — (a) UV–vis absorption spectra of TPE-1 (1 X 10^{-5} M), and (b) fluorescence spectra (λ_{ex}=360 nm) of TPE-1 in various solvents at room temperature respectively.

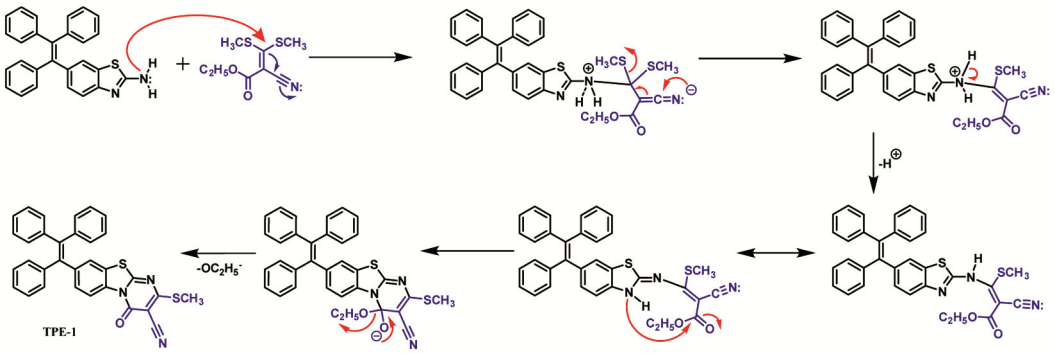

Scheme 2 — Proposed Reaction Mechanism Pathway for the Formation of TPE-1.

also found at 453 nm. As the solvent polarity shifted from MCH to $CHCl_3$~DCM, there was an initial increase in the fluorescence intensity of TPE-1, followed by a decrease when progressing to ACN and MeOH, and ultimately, the fluorescence completely diminished in DMSO, as illustrated in Fig. 2b. It provides information about TPE-1 molecular architecture whose fluorescence is highest in the medium polarity solvents. These fluorescence properties are ascribed to the suppression of the proximity effect (SOPE), which is exhibited by carbonyl and nitrogen bearing heterocyclic compounds[38-39].Thus, our TPE-1 molecular design exhibited nonmonotonic responses to polarity stimuli.

AIE characteristics of TPE-1

The AIE characteristics of compound TPE-1 was investigated using UV-Vis and fluorescence emission experiments in DMSO and DMSO/H_2O solvent mixture with varying volume (0-95%) of water fraction. The AIE property results were shown in Fig. 3a, 3b and 3c. In DMSO, TPE-1 exhibited four peaks at 262 ($\varepsilon = 4.22 \times 10^4$ M^{-1} cm^{-1}), 308 nm ($\varepsilon = 2.55 \times 10^4$ M^{-1} cm^{-1}), 334 ($\varepsilon = 2.70 \times 10^4$ M^{-1} cm^{-1}) and 366 nm ($\varepsilon = 3.31 \times 10^4$ M^{-1} cm^{-1}) (Fig. 3a). UV-Vis spectra displayed small decrease in peaks intensity at 308 nm ($\varepsilon = 2.84 \times 10^4$ M^{-1} cm^{-1}), 334 nm ($\varepsilon = 2.92 \times 10^4$ M^{-1} cm^{-1}), and 362 nm ($\varepsilon = 3.7 \times 10^4$ M^{-1} cm^{-1}), under H_2O at 40% volume fraction. When H_2O was further added up to $f_w \sim 50\%$, the peaks were shifted bathochromically and appeared at 257 nm ($\varepsilon = 4.48 \times 10^4$ M^{-1} cm^{-1}), 312 nm ($\varepsilon = 2.79 \times 10^4$ M^{-1} cm^{-1}), and 370 nm ($\varepsilon = 3.13 \times 10^4$ M^{-1} cm^{-1}) with decrease in intensity. Further, increase in f_{water} to 95%, the peaks were appeared at 256 nm ($\varepsilon = 4.75 \times 10^4$ M^{-1} cm^{-1}), 308 nm ($\varepsilon = 2.57 \times 10^4$ M^{-1} cm^{-1}), and 355 nm ($\varepsilon = 2.49 \times 10^4$ M^{-1} cm^{-1}) with significant change in intensities. The UV-Vis absorption spectra of TPE-1 are less sensitive to change in the different volume ratio of water in DMSO.

The aggregation induced emission (AIE) properties of TPE-1 was examined in DMSO with the addition of different water volume (0-95%) (Fig. 3b). When excited at 360 nm, TPE-1 exhibited a very weak emission peak at 542 nm in pure DMSO. The addition of water in increasing fractions from 10 to 30% did not significantly alter the emission peak. However, with a 40% water fraction (f_w), a small peak at 450 nm emerged. The emission intensity doubled when the water fraction was increased to 50%. A notable enhancement in emission intensity, approximately tenfold, was observed with 60 to 80% water fractions, where the peak appeared at 490 nm. This significant increase in emission intensity is attributed to the aggregation of TPE-1, as shown in Fig. 3b, which is ascribed to the AIE phenomenon. Conversely, upon adding 90% and 95% water, a decrease in the fluorescence peak intensity was noted, indicating the

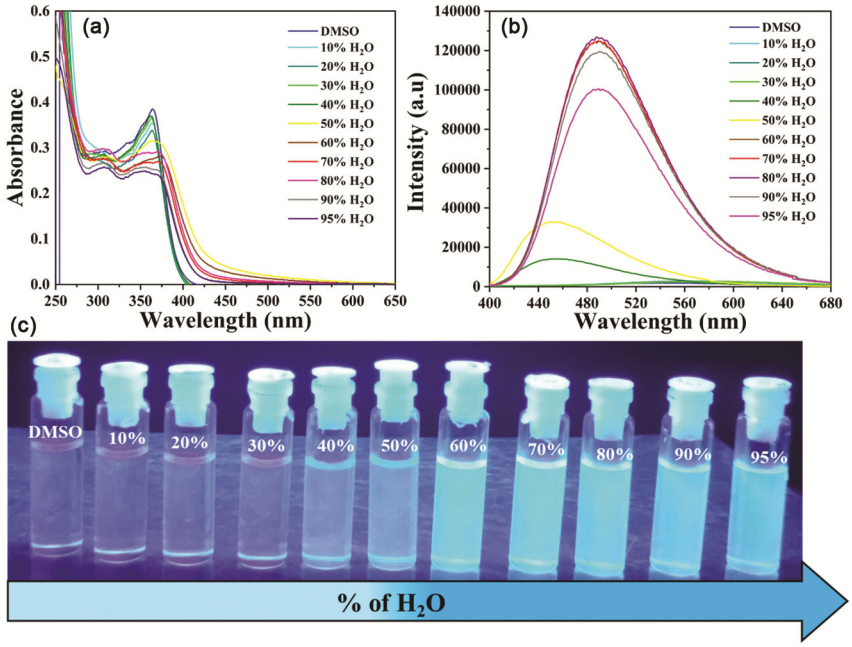

Fig. 3 — (a) UV–vis absorption spectra (b) fluorescence spectra (λ_{ex}=360 nm) of TPE-1 (1 X 10^{-5} M) in DMSO: H_2O with varying%'s of H_2O at room temperature respectively, and (c) necked eye images of TPE-1 in DMSO: H_2O (10:90) at room temperature respectively.

precipitation of TPE-1. The bathochromic shift in the fluorescence peak, correlating with increasing water fraction from 60 to 95%, is attributed to the formation of various aggregate states[40].The AIE properties of TPE-1 was also confirmed by recording quantum yield, which was increased from ϕ = 1.92% (DMSO) to 85.63% for water fraction of 90%. Thus, for f_w 90%, the fluorescence emission was dramatically enhanced, which was about 100-fold higher than that of TPE-1 in DMSO. The notable enhancement in emission intensity confirms the aggregation-induced emission (AIE) property[41] of TPE-1. This increase in emission properties are attributed to the restriction of intramolecular rotation (RIR) caused by the addition of water, which inhibits the free rotation of the phenyl ring system within the molecule[42,43].Furthermore, the photographic image of TPE-1 in DMSO and DMSO: water (0- 95%) solvent mixture under 365 nm UV light also confirmed the AIE properties of TPE-1 (Fig. 3c).

Mechanochromic Property of TPE-1

The mechanochromic characteristic of TPE-1 was studied to investigate color variation upon mechanical action. As displayed in Fig. 4, the TPE-1 powder exhibited deep blue color under 254 nm as well as 365 nm. TPE-1 upon grinding with pestle and mortar, the deep-blue color changed into deep green. These color change results monitored under 254 and 365 nm wavelength exhibited that highly ordered TPE-1 structure was disturbed upon the anisotropic grinding. The color change with mechanical grinding from deep blue to deep green could be completely restored by annealing at 150°C and fuming in acetone. Thus, the

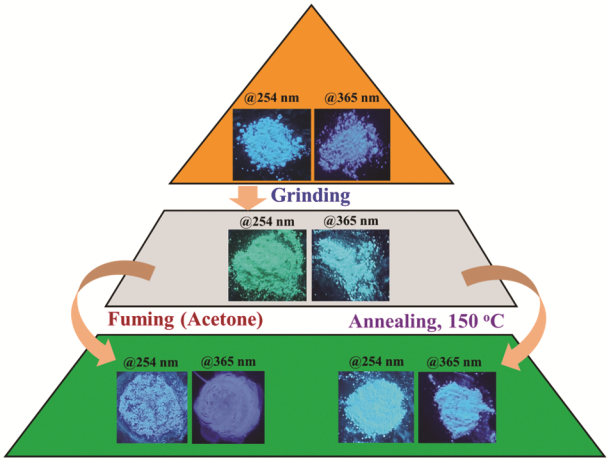

Fig. 4 — Mechanochromic characteristic of TPE-1 and the recovery of color after fuming by treating acetone and annealing at 150 °C under 254 nm and 365 nm.

reversible TPE-1 color change demonstrated the excellent TPE-1 crystallizability properties. Herein, we presume that such material is important for optical sensing applications.

Detection of Fe^{3+} in Solution

Further, to display the application of TPE-1, AIE active materials for recognition of metal ions, we investigated the fluorescence behaviour of TPE-1 towards different metal ions *e.g.* Hg^{2+}, Co^{2+}, Ni^{2+}, Ba^{2+}, Cd^{2+}, Fe^{3+}, In^{3+}, Mn^{2+}, Cr^{3+}, Mg^{2+}, Zn^{2+} and Cu^{2+}. The fluorescence measurements of TPE-1 (1×10^{-5} M) was carried out in DMSO: H_2O (10:90, v/v ratio) (Fig. 5). As shown in Fig. 5a, before addition of metal ions, TPE-1 emitted a strong fluorescence peak at 542 nm in DMSO: water (f_w = 90%). Among the tested metal ions (Hg^{2+}, Co^{2+}, Ni^{2+}, Ba^{2+}, Cd^{2+}, Fe^{3+}, In^{3+}, Mn^{2+}, Cr^{3+}, Mg^{2+}, Zn^{2+} and Cu^{2+}), the fluorescence emission peak intensity was significantly decreased with the addition of 80 equiv. of Fe^{3+} ions (Fig. 5a). The percentage quenching for TPE-1 in the presence of Fe^{3+} ion was 70% (Fig. 5b). Such significant fluorescence emission changes were not observed in the case of other metal cations (Fig. 5a and Fig. 5b). The significant decrease in TPE-1 fluorescence intensity with the addition of Fe^{3+} ions was ascribed to the interaction of TPE-1 ring nitrogen and sulphur with Fe^{3+} ions. In addition, colorimetric responses of TPE-1 to the metal cations were investigated at a 100 equiv. concentration of each under 365 nm light source. The color of TPE-1 solutions in DMSO: H_2O (10:90, *v/v* ratio) in the presence of these metal cations remains unaltered under the given experimental conditions at room temperature, except for the Fe^{3+} ion (Fig. 5c). The full bright blue color of TPE-1 turned to off green in the presence of Fe^{3+} ions (Fig. 5c). It is notable that the influence of other metal ions at high concentrations such as 100 equiv., 200 equiv, 300 equiv. and 500 equiv. unable to produce such color changes of TPE-1 solution (Fig. S12).

To get detailed insight about the efficiency of TPE-1 towards detection of Fe^{3+} ion, we performed fluorescence titration experiments. As exhibited in Fig. 6a, upon progressive addition of Fe^{3+} ions (0- 80 equiv.), the gradual decrease in the fluorescence intensity of TPE-1 was observed, suggesting complexation of Fe^{3+} with the receptor. The quenching efficiency of TPE-1 in the presence of Fe^{3+} ions was evaluated using the Stern-Volmer plot (Fig. 6b) and the Stern-Volmer equation. The Stern-Volmer plot for TPE-1 with Fe^{3+} showed a linear

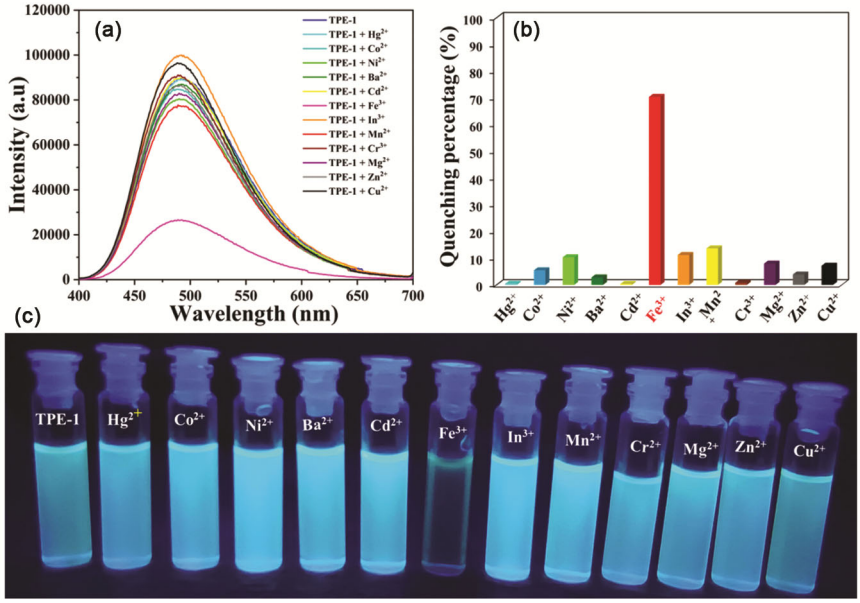

Fig. 5 — Fluorescence emission spectra (λ_{ex}= 360 nm) of TPE-1 (1 × 10^{-5} M) in DMSO: H_2O (1:9) (a) addition of 80 equiv. of various metals; (b) quenching percentage of TPE-1 upon the addition of various analytes respectively; (c) naked eye images of TPE-1 with 100 equiv. of various metals ions in DMSO: H_2O (10:90) at room temperature respectively.

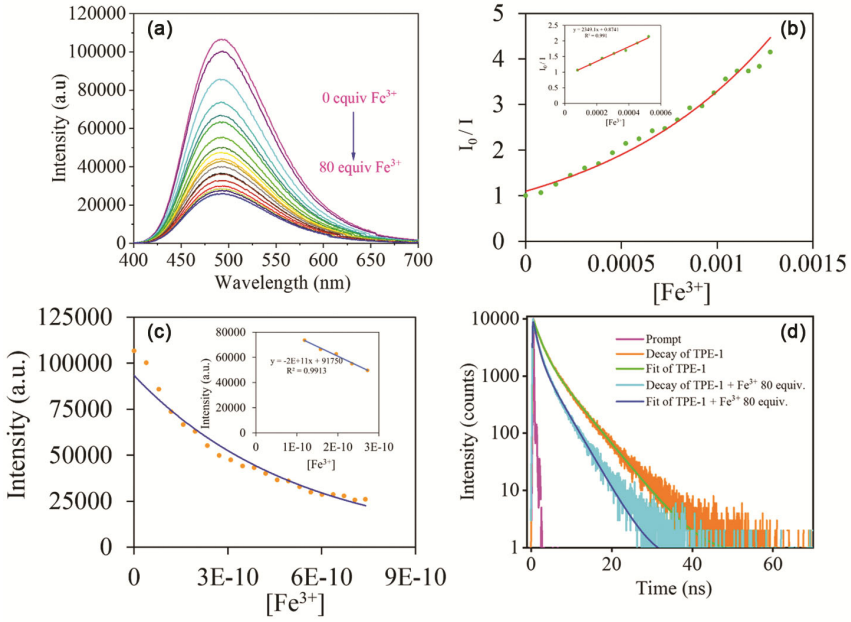

Fig. 6 — (a) Fluorescence emission spectra (λ_{ex}=360 nm) of TPE-1 (1 x10^{-5} M) in DMSO: H_2O (1:9) in the presence of Fe^{3+} ion (80 equiv.); (b) Stern−Volmer plot for TPE-1 with concentration of Fe^{3+} using emission of 493 nm (c) calibration curve of TPE-1 *versus* increasing concentration of Fe^{3+}; (d) TCSPC measurements of TPE-1 (1 × 10^{-5} M) and TPE-1 (1 × 10^{-5} M) + 80 equiv. of Fe^{3+} ions in DMSO-H_2O (f_{water} = 90%).

relationship in fluorescence intensity at lower concentrations of Fe^{3+}, while at higher concentrations, the plot exhibited an upward bend. This pattern suggests that the mechanism behind the fluorescence quenching of TPE-1 in the presence of Fe^{3+} ions is predominantly due to complex formation, rather than collisional deactivation. The estimated Stern-Volmer constant was found to be 2.34 × 10^3 M^{-1}, suggesting the high sensitivity of TPE-1 towards Fe^{3+} ions in the complex formation of TPE-1 with Fe^{3+} ion.The lower limit of detection of TPE-1 for Fe^{3+} was calculated using the calibration curve (Fig. 6c) and an equation 3σ/S. The evaluated LOD was found to be 1.02 × 10^{-7} M (102 nM). Therefore, TPE-1 receptor has great

potential for quantitative estimation of the Fe^{3+} ion concentration. To get in detail about the fluorescence quenching mechanism of TPE-1 up on addition of Fe^{3+} ions, TCSPC measurements were carried out and the results were depicted in Fig. 6d.

TCSPC measurements

Multiexponential functions are used to fit the decay traces according to the equations 1 and 2,

$$I(t) = I(0)\sum \alpha_i \exp(-t/\tau_i) \quad \ldots(1)$$

Also, the average fluorescence lifetime is calculated using

$$\tau_{avg} = \sum A_i\tau_i \; where \; A_i = \alpha_i\tau_i / \sum \alpha_i\tau_i \quad \ldots(2)$$

The excited-state lifetime of TPE-1 was analyzed in different environments: DMSO, a DMSO: H_2O mixture (water fraction = 90%), and in the presence of Fe^{3+} in a DMSO: H_2O mixture (water fraction = 90%). This analysis was conducted through biexponential fitting of the excited-state decay traces, as shown in Fig. S13 and Fig. 6d, with the decay time constants summarized in Table 1. The decay traces fitting revealed multiple lifetime components, such as τ_1 and τ_2, indicating the presence of diverse emissive characteristics in their excited state. The measurements for TPE-1 in DMSO (Fig. S13) showed rapid decay kinetics, with an average excited-state lifetime (τ_{avg}) of 0.41 ns. This suggests that non-radiative decay processes are predominant in this environment. In contrast, TPE-1 in the DMSO-H_2O mixture (f_w = 90%) exhibited a significantly longer τ_{avg} of approximately 4.67 ns (Fig. 6d, Table 1), which is considerably higher than in pure DMSO. This extended lifetime is attributed to the AIE properties of TPE-1, where the non-radiative pathways are reduced in the aggregated state induced by a higher volume of water. Furthermore, in the presence of Fe^{3+} ions, TPE-1 in the DMSO-H_2O mixture (f_w = 90%) demonstrated a τ_{avg} of 3.11 ns (Fig. 6d, Table 1), indicating a noticeable quenching effect. These excited-state lifetime results, combined with steady-state emission measurements, suggest that both dynamic and static quenching mechanisms are involved in the process.

Selective recognition of Fe^{3+} ions

Furthermore, to examine the practical applicability of the receptor TPE-1 as selective Fe^{3+} sensor over other interfering metal ions, competitive measurements were carried out in the presence of Fe^{3+} ions (80 equiv.) mixed with different metal ions including Hg^{2+}, Co^{2+}, Ni^{2+}, Ba^{2+}, Cd^{2+}, In^{3+}, Mn^{2+}, Cr^{3+}, Mg^{2+}, Zn^{2+} and Cu^{2+} ions (80 equiv.) in DMSO: H_2O (10:90, *v/v* ratio). The results are depicted in Fig. 7a and 7b. The fluorescence emission data revealed that the presence of other metal ions did not significantly affect the fluorescence (FL) peak

Table 1 — Excited-state lifetime components of TPE-1 (DMSO), TPE-1 (DMSO- H_2O, f_{water} = 10:90) and TPE-1 + Fe^{3+} 80 equiv. (DMSO- H_2O, f_{water} =10:90)

Sample	a_1	τ_1 (ns)	a_2	τ_2 (ns)	τ_{avg} (ns)	χ^2
TPE-1 (DMSO)	86.39	0.111	13.61	0.709	0.411	1.44
TPE-1 (DMSO-H_2O 10:90)	42.11	1.602	57.89	5.077	4.673	1.42
TPE-1 + Fe^{3+} 80 equiv. (DMSO-H_2O 10:90)	44.79	0.966	55.21	3.58	3.110	1.70

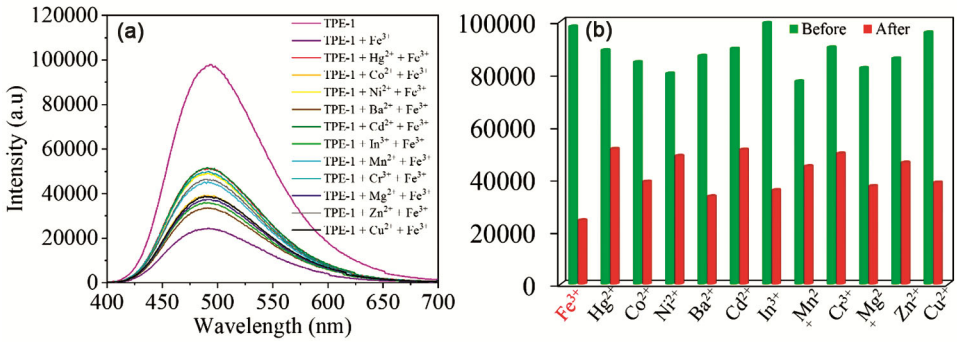

Fig. 7 — (a) TPE-1 with Fe^{3+} in presence of other metals analytes; (b) bar graph plots (green color bar represents TPE-1 + respective metal ions and red color bar represents TPE-1 + respective metal ions + Fe^{3+} ions) shows changes of fluorescence emission intensity of TPE-1 towards Fe^{3+} in presence of other metals analytes (80 equiv.) respectively.

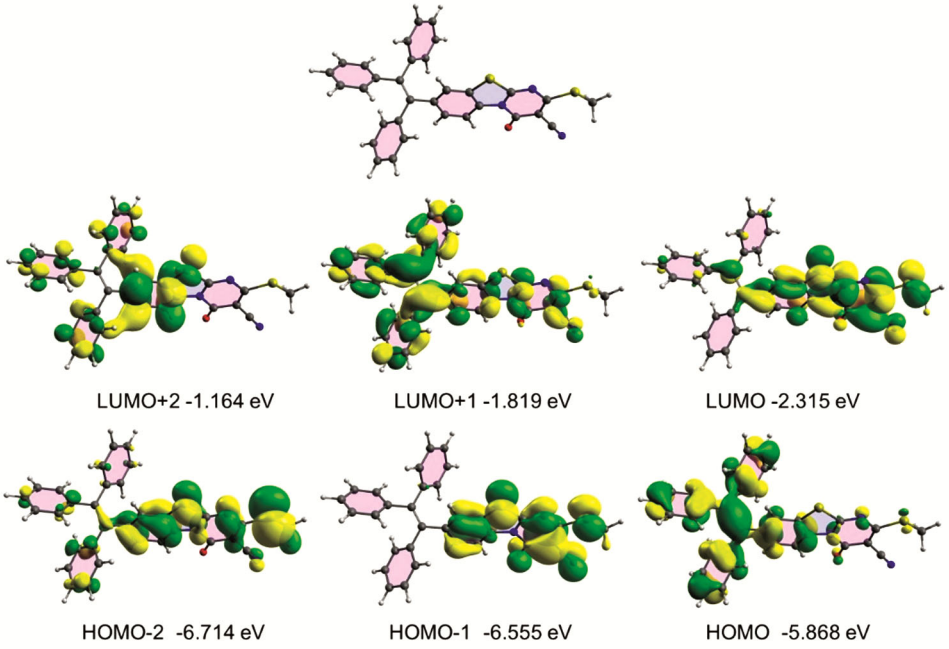

Fig. 8 — The frontier molecular orbitals including HOMO and LUMO of L, as calculated using DFT at B3LYP def2-SVP def2/J level of theory.

intensity of the sample. This observation was consistent when comparing the FL peak intensities with and without the presence of interfering metal cations. These results suggested that the receptor TPE-1 can be utilized to detect selectively Fe^{3+} ions in environmental and real world applications.

Computational study

Theoretical *in vacuo* geometry optimization, density functional theory (DFT), complete active space self-consistent-field (CASSCF) and time dependent density functional theory (TDDFT) calculations were performed using the ORCA (Version 5.0.3) software package[32]. The highest occupied molecular orbital (HOMO) and lowest unoccupied molecular orbital (LUMO) energy levels are displayed in Fig. 8.

To reduce the simulation cost, a truncated form of the ligand was considered for the iron complexes modelling. The geometry optimization was initiated from position (A) ended in the final confirmation of (B), indicating that the methyl thiol moiety is more available for complexing with iron (Fig. 9).

CASSCF and second-order *N*-electron valence perturbation theory (NEVPT2) methods were used to take into account the dynamic correlations. The chosen active space consisted of the five d electrons of the iron d orbitals which are involved in the

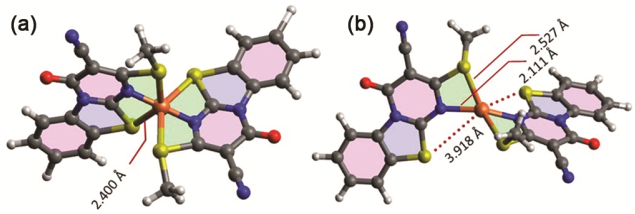

Fig. 9 — The geometry optimization of the interaction between the ligand and Fe^{3+}.

complexing interactions. The DFT was conducted at B3LYP def2-SVP def2/J level of theory, and the CASSCF was conducted at RIJCOSX def2-SVP def2-svp/c def2/J level of theory[33].

The geometry optimization of the Fe^{3+}: L2 and Fe^{3+}: L3 complexes with two ligands to one Fe^{3+} and three ligands to one Fe^{3+} starting the geometry conformations from square and octahedral crystal fields and ending with a geometry optimised structures with distorted tetrahedral and octahedral ligand fields respectively (Fig. 10a and b). The DFT modelling of the Fe^{3+}: L2 and Fe^{3+}: L3 shows that the d orbitals of the Fe^{3+} are interacting with the ligands MOs and their presence can be observed in the frontier HOMO orbitals of the Fe^{3+}: L2 complex (Fig. 10a), while the d orbitals of the Fe^{3+} in the Fe^{3+}:L3 complex (Fig. 10b) show less presence in the frontier MOs.

The CASSCF simulations were performed on the geometry optimised complex structures and used to

evaluate the d orbitals interaction with the ligands. The results show that the ligand field cause a greater d orbital splitting in octahedral Fe^{3+}: L3 compared to the distorted tetrahedral Fe^{3+}: L2 complex (see Table 2). Due to the asymmetric nature of L by being a bidentate ligand, resulting in an asymmetric distorted octahedral and tetrahedral ligand fields, the d orbitals split into two groups in both cases that can

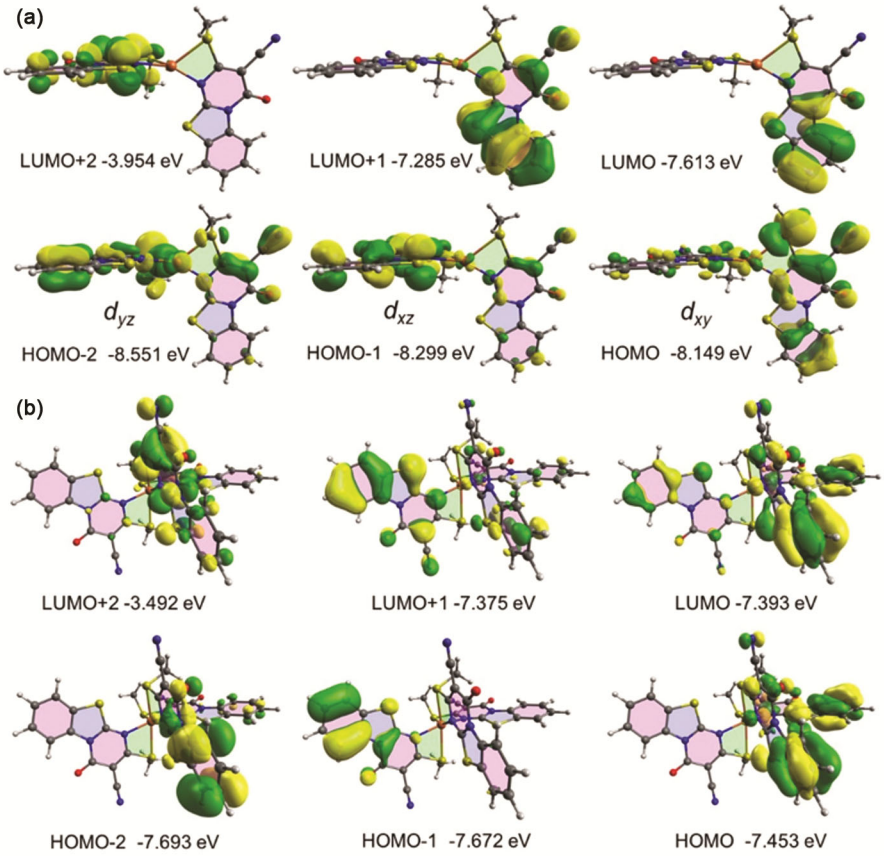

Fig. 10 — The frontier molecular orbitals including HOMO and LUMO of the truncated (a) Fe^{3+}: L2 and (b) Fe^{3+}: L3 complexes, as calculated using DFT at B3LYP def2-SVP def2/J level of theory.

Table 2—The frontier molecular orbitals energy states including HOMO, LUMO, HOMO – LUMO gap and HOMO → LUMO transition (photo-excitation) energy and oscillation strength of the L, and Fe^{3+}: L2 and Fe^{3+}: L3 complexes as calculated using DFT, TDDFT at B3LYP def2-SVP def2/J functionals, and CASSCF at RIJCOSX def2-SVP def2-svp/c def2/J level of theory.

	L	Truncated $Fe^{3+}L_2$	Truncated $Fe^{3+}L_2$	Truncated $Fe^{3+}L_3$	Truncated $Fe^{3+}L_3$
	TDDFT	DFT	CASSCF	DFT	CASSCF
L+5 (eV)	–0.726	–2.558	–7.447	–2.326	–6.155
L+4 (eV)	–0.815	–2.799	–8.485	–3.406	–7.526
L+3 (eV)	–1.121	–3.332	–8.515	–3.445	–7.628
L+2 (eV)	–1.164	–3.954	–8.967	–3.492	–7.740
L+1 (eV)	–1.819	–7.285	–16.798 (d_{z^2})	–7.375	–13.572 (d_{z^2})
L (eV)	–2.315	–7.613	–18.837 ($d_{x^2-y^2}$)	–7.393	–15.518 ($d_{x^2-y^2}$)
H (eV)	–5.868	–8.149	–24.335 (d_{xz})	–7.453	–21.952 (d_{xz})
H-1 (eV)	–6.555	–8.299	–24.628 (d_{yz})	–7.672	–22.495 (d_{yz})
H-2 (eV)	–6.714	–8.551	–25.369 (d_{xy})	–7.693	–22.921 (d_{xy})
H-3 (eV)	–7.075	–8.643	–16.698	–7.700	–16.423
H-4 (eV)	–7.153	–8.682	–17.176	–8.181	–16.555
H-5 (eV)	–7.344	–8.843	–17.276	–8.342	–16.572
$E_{HOMO-LUMO\ gap}$ (eV)	3.553	0.536	-	0.060	-
$\Delta\ d_{xz} \rightarrow d_{x^2-y^2}$(eV)	-	-	5.498	-	6.434
Wavelength (nm)	391.7	-			
f (Osc. Strength)	0.370643	-			

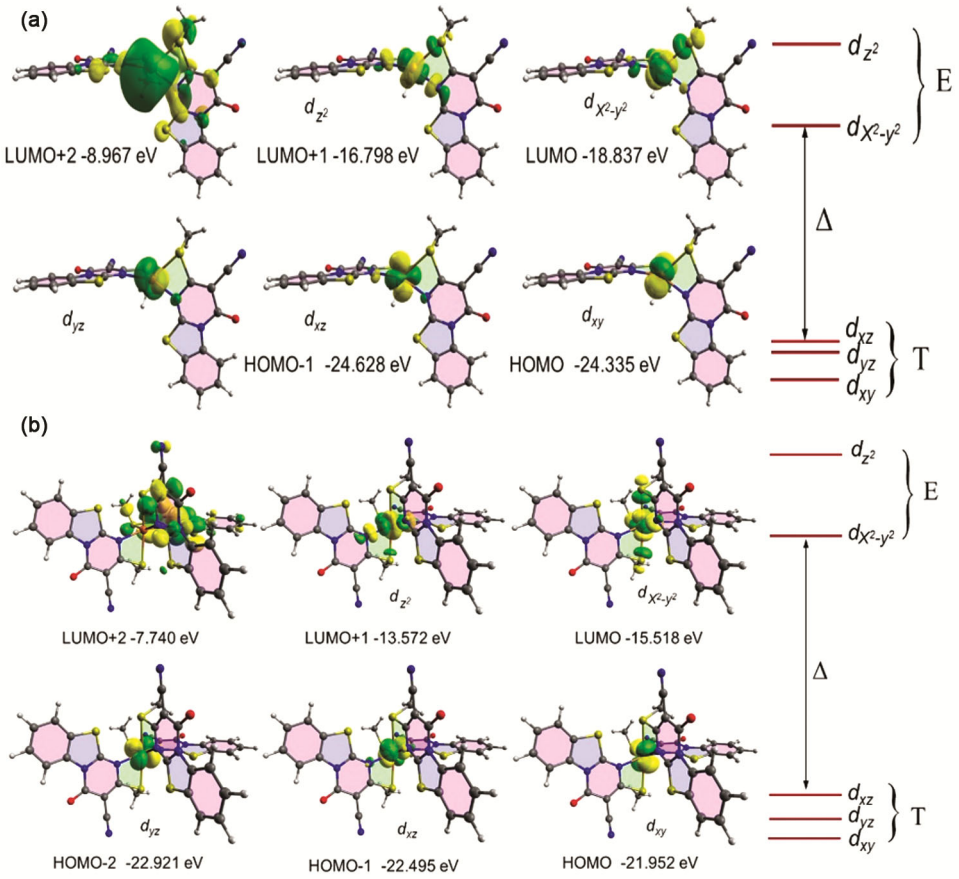

Fig. 11 — The frontier molecular orbitals in the active space of the truncated (a) Fe^{3+}:L2 and (b) Fe^{3+}: L3 complexes, as calculated using CASSCF at RIJCOSX def2-SVP def2-svp/c def2/J level of theory.

be compared to T and E electronic structures (Fig. 11). All d orbitals energy and symmetry were different. Table 2 shows the energy of the frontier orbitals and complex active space orbitals as calculated using DFT, TDDFT and CASSCF with NEVPT2 and QDPT corrections.

The DFT modelling study demonstrated that TPE-1 ligand MOs interacting with the d orbitals of the Fe^{3+}, confirming the experimental results of complexation between TPE-1 and Fe^{3+} ions.

Real-world applications

The TPE-1 receptor exhibited outstanding emission response characteristics and selective detection of Fe^{3+} ions, even in the presence of other metal ions, combined with an impressive detection limit. These qualities led to an exploration of its real-world applications. Specifically, TPE-1 was utilized to detect Fe^{3+} in various water samples, including distilled water, tap water, and lake water[44].The results of these water sample analyses are presented in Table 3. Initially, no Fe^{3+} ions were present in the examined water samples. Subsequently, concentrations of 2, 4, 6, and 8 μM of Fe^{3+} ions were added to the water samples containing 1×10^{-5} M of the TPE-1 receptor. Each sample underwent testing three times to ensure reliability. This experimental protocol for estimating Fe^{3+} ion concentrations in

Table 3—Real samples analysis in different water of Fe^{3+}.

Sample	Addition	Found $X^a \pm SD^b$ (μM)	Recovery (%)	RSD^c (%)
Distilled Water	2	1.9862±0.0150	99.31	0.75
	4	1.9862±0.0150	99.68	0.22
	6	5.994±0.0086	99.9	0.14
	8	7.9895±0.0163	99.86	020
Tap Water	2	1.9695±0.0274	98.47	1.39
	4	3.9868±0.0341	99.67	0.85
	6	5.9601±0.0086	99.35	0.14
	8	7.9953±0.0337	99.94	0.42
Lake Water	2	1.9545±0.0557	97.72	2.85
	4	3.9700±0.0403	99.25	1.01
	6	5.9587±0.0239	99.20	0.40
	8	7.9360±0.0094	99.68	0.11

water samples proved to be effective. Therefore, TPE-1 is demonstrated to be an excellent molecular architecture for the selective detection of Fe^{3+} ions in environmental samples.

X[a]: Mean of three determinations, SD[b]: Standard deviation, RSD[c]: Relative standard deviation. (Distilled water and Tap Water = CSIR-IICT Hyderabad, lake water from Hussain Sagar Hyderabad)

Comparison with previous results

A comparative detection limit of TPE-1 towards Fe^{3+} ion with previously literature reports are shown in Table 4. The comparison study showed that TPE-1

Table 4 — Comparison of chemosensors for selective recognition of Fe^{3+} ion.

Sr.No.	Targeted Analytes	Solvent System	Limit of detection	Reference
1.	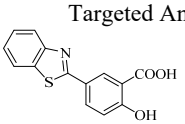 **Sensor 1**	CH_3CN: H_2O (4:1) DMF: H_2O (1:1)	8.43×10^{-6} M 5.86×10^{-6} M	45
2.	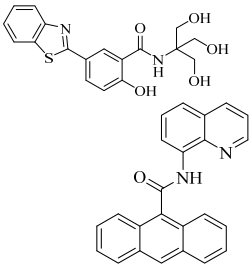 **HAQ**	DMSO	1.3×10^{-6} M	46
3.	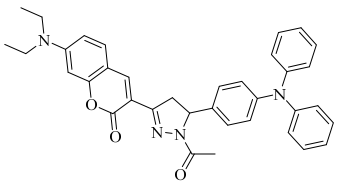 **A**	THF	1.01×10^{-7} M	47
4.	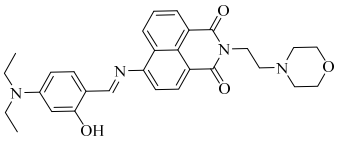 **NDSM**	CH_3CN: H_2O (7:3)	0.81 µM	48
5.	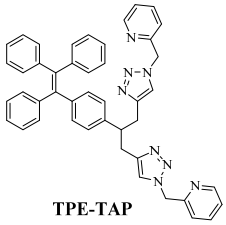 **TPE-TAP**	THF: H_2O (2:98)	1.3 µM	49
6.	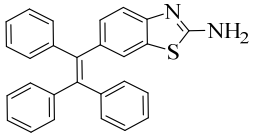	DMSO: H_2O (10:90)	1.74×10^{-7} M	28
7.	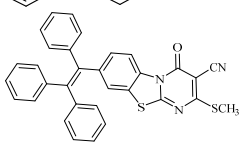 **TPE-1**	DMSO: H_2O (10:90)	1.02×10^{-7} M *i.e.* (102 nM)	This Work

exhibited the competitive lower detection limit for Fe^{3+} ions compared to the literature AIE sensors[29b, 45-49]. Thus, the present protocol for Fe^{3+} ion recognition using TPE-1 could be employed in practical applications as colorimetric and fluorescent sensor.

Conclusions

In summary, we report the synthesis and characterization of a novel AIE-active chromophore TPE-1, which incorporates a benzothiazole-pyrimidine unit with electron-donating and electron-withdrawing groups. TPE-1 exhibits remarkable photophysical properties, such as high thermal stability, non-monotonic solvatochromism, and mechanochromic. TPE-1 also demonstrates selective and sensitive detection of Fe^{3+} ions over other metal ions in DMSO-water mixtures, with a low limit of detection of 102 nM. The binding mechanism of TPE-1 with Fe^{3+} ions was investigated by computational calculations. The practical applicability of TPE-1 as a Fe^{3+} sensor is demonstrated by its successful detection of Fe^{3+} ions in various water samples, such as distilled water, tap water, and lake water. The manuscript presents a simple and efficient method for the design and development of a new AIE-active chromophore with potential applications in environmental and biological systems.

Acknowledgements

S.V.B. (IICT) is grateful for financial support from the DAE-BRNS under the project No. 58/14/01/2020-BRNS/37047, and IICT/Pubs./2024/01. D. I. B. acknowledges CSIR for senior research fellowship (SRF). S.V.B. (CUK) acknowledges University Grant Commission (UGC) financial support and Professorship under Faculty Recharge Programme (FRP).

Supplementary Information

Supplementary information is available in the website http://nopr.niscpr.res.in/handle/123456789/58776.

References

1 Woosley S E, Heger A & Weaver T A, *Rev Mod Phys,* 74 (2002) 1015.
2 Jordan T H, *Proc Natl Acad Sci U S A, 76* (1979) 4192.
3 Frey P A & Reed G H, *ACS Chem Biol*, 7 (2012) 1477.
4 Dai S, Schwendtmayer C, Schürmann P, Ramaswamy S & Eklund H, *Science*, 287 (2000) 655.
5 Beutler E, *Science*, 306 (2004) 2051.
6 Atkinson A & Winge D R,*Chem Rev*,109 (2009) 4708.
7 Kaplan C D & Kaplan J,*Chem Rev*,109 (2009) 4536.
8 Theil E C & Goss D J, *Chem Rev*,109 (2009) 4568.
9 Vona R, Pallotta L, Cappelletti M, Severi C & Matarrese P, *Antioxidants*, 10 (2021) 201.
10 Turan B A, *Biol Trace Elem Res*, 188 (2019) 160.
11 Bhutani P,Joshi G, Raja N ,Bachhav N, Rajanna P K, Bhutani H, Paul A T & Kumar R*, J Med Chem*, 64 (2021) 2339.
12 Pivina L, Semenova Y, Doşa M D, Dauletyarova M & Bjørklund G, *J Mol Neurosci*, 68 (2019) 1.
13 Timerbaev A R, Dabek-Zlotorzynska E & Marc V D H A G T, *Analyst,* 124 (1999) 811.
14 Gomes D C, Segundo M A, Lima J C & Rangel A S, *Talanta,* 66 (2005) 703.
15 Shamspur T, Sheikhshoaie I & Mashhadizadeh M H, *J Anal AtSpectrom,* 20 (2005) 476.
16 Lunvongsa S, Oshima M & Motomizu S, *Talanta,* 68 **(**2006) 969.
17 Vanloot P, Coulomb B, Brach-Papa C, Sergent M & Boudenne J L, *Chemosphere***,** 69 (2007) 1351.
18 Svechkarev D & Mohs A M, *Curr Med Chem*, 26 (2019) 4042.
19 Sahoo S K &Crisponi G, *Molecules*, 24 (2019) 3267.
20 Sui B, Tang S, Liu T, Kim B & Belfield K D, *ACS Appl Mat Interfaces*, 6 (2014) 18408.
21 Shylaja A, Rojam S S, Priya R V & Kumar R R, *J Org Chem*, 83 (2018) 14084.
22 Seenan S &Iyer S K, *J Org Chem*, 85 (2020) 1871.
23 Guo B, Liu Q, Su Q, Liu W, Ju P, Li G & Wu Q, *J Mat Sci*, 53 (2018) 15746.
24 Kang S, Han H, Leem K & Kim K M, *ACS Omega*, 7 (2022) 2074.
25 Nandhini T,Kaleeswaran P&Pitchumani K,*Sens Actuators B Chem*, 230 (2016) 199.
26 Jamuna K, Thimmarayaperumal S, Aravind M K, Sivakumar S &Ashokkumar B, *New J Chem*, 46 **(**2022) 9207.
27 Bhalla V, Gupta A & Kumar M, *Dalton Trans*, 42 (2013) 4464.
28 Bhusanur D I, Singh P K, Bhosale S V & Bhosale S V, *J Photochem Photobio A:Chem,* 449 (2024) 115357.
29 Meng X, Zhang D, Wang M, Zhao R, Zhang P, Zhao J & Deng K, *Poly Adv Tech*, 33 (2022) 4120.
30 La D D, Bhosale S V, Jones L A & Bhosale S V, *ACS Appl Mat Interfaces*, 10 (2018) 12189.
31 Lakowicz J R, In principles of fluorescence spectroscopy, 3rd ed., (Plenum; New York) 2006, p.278.
32 Neese F, *Rev Comp Mol Sci*, 8 (2018) e1327.
33 Lee C, Yang W & Parr R G, *Phys Rev B, Condens Matt*, 37 (1988) 785.
34 Goel A, Chaurasia S, Dixit M, Kumar V, Prakash S, Jena B, Verma J K, Jain M, Anand R S & Manoharan S S, *Org Lett*, 11 (2009) 1289.
35 More K S, Mirgane H A, Shaikh S, Perupogu V, Birajdar S S, Puyad A L, Bhosale S V & Bhosale S V, *J Org Chem*, 89 (2024) 5917.
36 Baheti K G, Kapratwar S B & Kuberkar S V, *Syn Comm*,32 (2002) 2237.
37 Yuan W Z,Gong Y,Chen S,Shen X Y, Lam J W,Lu P, Lu Y, Wang Z, Hu R,Xie N, Kwok S H, Zhang Y, Sun J Z & Tang B Z, *Chem Mat*, 24 (2012) 1518.
38 Lai T I, Lim B T & Lim E C, *J Am Chem Soc*, 104 (1982) 7631.

39 Tu Y, Yu Y, Xiao D, Liu J, Zhao Z, Liu Z, Lam J W Y & Tang B Z, *AdvSci,*7 (2020) 2001845.

40 Zhang X, Chi Z, Xu B, Chen C, Zhou X, Zhang Y, Liu S & Xu J, *J Mat Chem*, 22 (2012) 18505.

41 Saravanan E, Sathishkumar M, Sathiyanathan P, Dhanapal J, Selin M K &Kulathu I S, *Talanta*, 264 (2023) 124726.

42 Hong Y, Lam J W Y & Tang B Z, *Chem Comm***,** (2009) 4332.

43 Mei J,Hong Y, Lam J W Y,Qin A, Tang Y & Tang B Z, *Adv Mater*, 26 (2014) 5429.

44 Xu Z, Shi W, Yang C, Xu J, Liu H, Xu J & Zhu B, *RSC Adv*, 9 (2019) 10554.

45 Gong X, Ding X, Jiang N, Zhong T & Wang G, *Microchem J,* 152 (2020) 1043514.

46 Tehrani T, Meghdadi S, Salarvand Z, Tavakoli B, Eskandari K &Amirnasr M, *New J Chem,* 45 (2021) 8109.

47 Zhang Y P, Teng Q, Yang Y S, Guo H C & Xue J J, *Inorganica Chim Acta*, 525 (2021) 120469.

48 Jothi D, Munusamy S, Sawminathan S & Iyer S K, *RSC Adv,* 11 (2021) 11338.

49 Dalkilic O, Bozkurt E L F & Kilic H, *Org Biomol Chem*, 21 (2023) 5406.